JACC: BASIC TO TRANSLATIONAL SCIENCE VOL. 5, NO. 10, 2020

PRECLINICAL RESEARCH

Proteolysis of Von Willebrand Factor Influences Inflammatory Endothelial Activation and Vascular Compliance in Atherosclerosis

Koya Ozawa, MD, PhD,[a] Matthew A. Muller, BS,[a] Oleg Varlamov, PhD,[b] Hagai Tavori, PhD,[a] William Packwood, BS,[a] Paul A. Mueller, PhD,[a] Aris Xie, MS,[a] Zaverio Ruggeri, MD,[c] Dominic Chung, PhD,[d] José A. López, MD,[d] Jonathan R. Lindner, MD[a,b]

VISUAL ABSTRACT

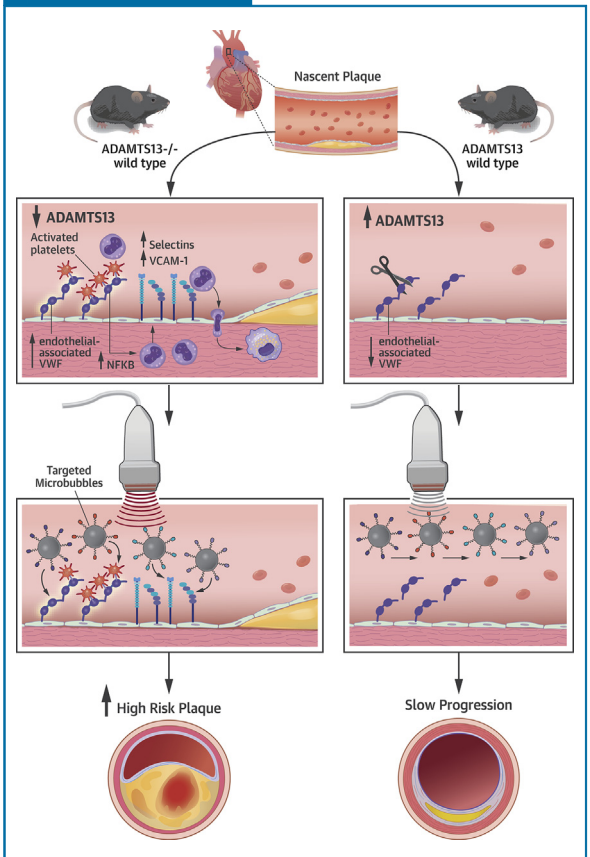

Ozawa, K. et al. J Am Coll Cardiol Basic Trans Science. 2020;5(10):1017–28.

HIGHLIGHTS

- **In murine models of atherosclerosis, excess endothelial-associated vWF results not only in platelet adhesion, but also endothelial expression of leukocyte adhesion molecules, indicating a role of platelets in endothelial activation.**
- **The events triggered by excess endothelial-associated vWF lead to accelerated plaque growth and abnormal arterial mechanical properties.**
- **The cellular and molecular events described herein can be assessed noninvasively through molecular imaging.**

From the [a]Knight Cardiovascular Institute, Oregon Health and Science University, Portland, Oregon; [b]Oregon National Primate Research Center, Oregon Health and Science University, Portland, Oregon; [c]Department of Molecular and Experimental Medicine, Scripps Research Institute, La Jolla, California; and the [d]Bloodworks Research Institute, Seattle, Washington.

ISSN 2452-302X https://doi.org/10.1016/j.jacbts.2020.08.009

ABBREVIATIONS AND ACRONYMS

AD13$^{-/-}$ = deficient for ADAMTS13

Apo-E$^{-/-}$ = deficient for apolipoprotein-E

BP = blood pressure

GPIbα = glycoprotein-Ibα

LDL = low-density lipoprotein

LDL-R = low-density lipoprotein receptor

LDL-R$^{-/-}$ = deficient for low-density lipoprotein receptor

MB = microbubble

NFκB = nuclear factor κ-light-chain-enhancer of activated B cells

vWF = von Willebrand factor

WSD = Western-style diet

SUMMARY

This study used in vivo molecular imaging to characterize endotheliall activation attributable to von Willebrand factor (vWF)-mediated platelet adhesion in atherosclerosis. In atherosclerotic mice lacking the low-density lipoprotein receptor on Western diet, the additional genetic deletion of the ADAMTS13, which cleaves endothelial-associated vWF, produced greater aortic molecular imaging signal for not only vWF and platelets, but also for endothelial adhesion molecules VCAM1 and P-selectin, larger plaque size, and lower aortic distensibility. Sustained ADAMTS13 therapy reduced signal for all 4 molecular targets and plaque size. We conclude that excess endothelial-associated vWF contributes to not only platelet adhesion, but also to up-regulation of endothelial cell adhesion molecules. (J Am Coll Cardiol Basic Trans Science 2020;5:1017–28)

In atherosclerosis, cytokine-mediated cell activation and expression of endothelial cell adhesion molecules contribute to the innate immune response (1). Platelet-endothelial interactions have also been shown to promote plaque development even at early stages of disease, most likely through proinflammatory effects of the platelet secretome, direct effects on macrophage subtype, or by serving as an alternative binding partner for leukocytes (2–9). In vivo molecular imaging has recently been used to confirm histological findings that arterial platelet adhesion in atherosclerosis is mediated by increased endothelial-associated von Willebrand factor (vWF) and exposure of the vWF A1 binding domain for the glycoprotein-Ibα (GPIbα) subunit of the platelet GPIb-IX-V complex (10–12). Accumulation of self-associated vWF on the endothelium in atherosclerosis has been attributed in part to impaired cleavage by ADAMTS-13 (12–14).

In these models, chronic inhibition of GPIbα or genetic deficiency of endothelial vWF reduces plaque size and macrophage content (5,15), whereas genetic deficiency of ADAMTS13 increases plaque size (15,16). Mechanistically, platelets not only secrete a wide variety of proinflammatory molecules, but they are also capable of endothelial deposition of chemokines such as CCL5 (4,6). Yet, little is known about in vivo endothelial activation from platelet adhesion except that hyperlipidemic mice deficient in vWF have reduced expression of P-selectin, possibly reflecting their shared storage in endothelial Weibel-Palade bodies, and less leukocyte arterial adhesion (14,15).

In this study, we hypothesized that excess endothelial-associated vWF, which can promote platelet adhesion in early atherosclerosis, directly leads to proinflammatory endothelial activation evidenced through adhesion molecule expression and to changes in vascular compliance. To test our hypothesis, we used in vivo molecular imaging of endothelial vWF, platelet adhesion, and adhesion molecules to temporally characterize arteries in atherosclerosis-prone mice, which are produced by deletion of the low-density lipoprotein receptor (LDL-R$^{-/-}$) and a Western-style diet (WSD), with and without genetic deletion of ADAMTS13. Effects of acute and sustained recombinant ADAMTS13 therapy on endothelial adhesion molecular expression were also tested.

METHODS

ANIMAL MODELS. The study was approved by the Animal Care and Use Committee at Oregon Health and Science University and all procedures conformed to National Institutes of Health Guide for the Care and Use of Laboratory Animals. Mouse strains used included wild-type C57BL/6 mice, LDL-R$^{-/-}$ mice, and mice deficient for both LDL-R and ADAMTS13 (LDL-R$^{-/-}$AD13$^{-/-}$). Mice were fed either a normal chow diet or, starting at 14 weeks of age, a WSD containing 21% fat by weight (15% saturated fat) contributing to 42% of caloric intake (Teklad

The authors attest they are in compliance with human studies committees and animal welfare regulations of the authors' institutions and Food and Drug Administration guidelines, including patient consent where appropriate. For more information, visit the *JACC: Basic to Translational Science* author instructions page.

Manuscript received June 2, 2020; revised manuscript received August 26, 2020, accepted August 26, 2020.

TABLE 1 Plasma Lipid Concentrations in Mice at 30 Weeks of Age

	WT (n = 6)	LDL-R$^{-/-}$ (n = 8)	LDL-R$^{-/-}$ + WSD (n = 8)	LDL-R$^{-/-}$ AD13$^{-/-}$ + WSD (n = 6)
Total cholesterol, mg/dl	56 ± 8	193 ± 57*	999 ± 273†	1,000 ± 284†
HDL cholesterol, mg/dl†	38 ± 8	42 ± 14	62 ± 16	55 ± 16
LDL cholesterol, mg/dl	7 ± 2	114 ± 30*	552 ± 167†	516 ± 180†
Triglycerides, mg/dl	35 ± 10	94 ± 58*	697 ± 293†	690 ± 210†

Values are mean ± SD. *p < 0.01 versus WT mice; †p < 0.01 versus WT and LDL-R$^{-/-}$ mice (corrected for multiple comparisons).
AD13$^{-/-}$ = deficient for ADAMTS13; HDL = high-density lipoprotein; LDL = low-density lipoprotein; LDL-R$^{-/-}$ = deficient for low-density lipoprotein receptor; WSD = Western-style diet; WT = wild type

TD.88137; Envigo, Huntingdon, United Kingdom). Mice were studied at 20 and 30 weeks of age. Additional cohorts of 30-week-old LDL-R$^{-/-}$ mice on WSD were studied: 1) after treatment with recombinant human ADAMTS13 (5 μg intravenously) (R and D Systems, Minneapolis, Minnesota) given 1 h prior to molecular imaging; or 2) after treatment for the preceding 14 days with ADAMTS13 administered by osmotic minipump (1004, Alzet, Cupertino, California) placed subcutaneously and loaded at 0.75 mg/ml of ADAMTS13 to release 2 μg/day. Activity of human ADAMTS13 against murine vWF has been validated previously using platelet binding assays in shear (12). Mice were anesthetized with inhaled isoflurane (1.0% to 2.0%) and, when required, a catheter was placed in a jugular vein for administration of contrast agent or drugs. Euthanasia at the completion of study was performed with by inhaled anesthetic overdose (isoflurane 5%) together with cervical dislocation.

LIPID ANALYSIS. For lipid measurements, serum samples were analyzed in duplicate using liquid reagents for cholesterol (Pointe Scientific, Canton, Michigan) or triglycerides (Pointe Scientific), respectively. Absorbance was measured at 490 nm for cholesterol and at 540 nm for triglycerides using a microplate reader (SpectraMax iD3, Molecular Devices, San Jose, California) using cholesterol and glycerol standards (Pointe Scientific). Pooled samples with equal contributions from each animal were used to measure high-density lipoprotein and direct LDL cholesterol using commercially available reagents (Randox Laboratories, Crumlin, United Kingdom) and a chemistry analyzer (Hitachi 704; Roche Diagnostics Corp., Indianapolis, Indiana).

MOLECULAR IMAGING PROBES. Microbubbles (MBs) targeted to endothelial vWF (MB_{vWF}), GPIbα as an indicator of platelet adhesion (MB_{Plt}), VCAM1 (MB_{VCAM}), and P-selectin (MB_{Sel}) were prepared as follows. Biotinylated lipid-shelled decafluorobutane MBs were created by sonication of a gas-saturated aqueous lipid dispersion of distearoylphosphatidylcholine (2 mg/ml), polyoxyethylene-40-stearate (1 mg/ml), and distearoylphosphatidylethanolamine-polyethyleneglycol [PEG] (2000)-biotin (0.4 mg/ml). Surface conjugation of biotinylated ligands was performed as previously described using the following ligands: 1) a cell-derived biotinylated peptide representing the soluble N-terminal 300 amino acids of GPIbα with gain-of-function D235Y and M239V mutations for MB_{vWF} (17); 2) dimeric recombinant murine vWF A1 domain (mature vWF amino acids 445 to 716) for MB_{Plt}; and 3) monoclonal antibodies against the extracellular domain of either murine VCAM1 (clone 429, BD Biosciences, San Jose, California) or P-selectin (RB40.34, BD Biosciences) for MB_{VCAM} and MB_{Sel}, respectively (12,18). Specificity for each agent for their intended target has been previously validated (12,18). Control nontargeted MBs were prepared without distearoylphosphatidylethanolamine-PEG(2000)-biotin. For each experiment, electrozone sensing (Multisizer III, Beckman Coulter, Brea, California) was used to measure MB concentration and to ensure similar size distribution between agents.

MOLECULAR IMAGING OF THE THORACIC AORTA. Molecular imaging was performed at 20 and 30 weeks of age (n = 7 to 12 animals for each group and each molecular target at 20 weeks; n = 8 to 13 animals for each group and each molecular target at 30 weeks). Imaging was performed with a linear-array probe transducer (15L8) interfaced with an ultrasound system (Sequoia, Siemens Medical Systems, Mountain View, California). Contrast-specific power-modulation pulse-inversion imaging was performed at a centerline frequency of 7 MHz, a dynamic range of 50 dB, and a mechanical index of 0.97. Gain was set at a level that eliminated pre-contrast background speckle and kept constant. The ascending aorta was imaged in long-axis gated to end-diastole. Images were acquired 8 min after intravenous injection of 1×10^6 targeted or control MBs administered in random order. Signal intensity from adherent MBs was determined by acquiring the first frame and then digitally subtracting averaged frames obtained after complete destruction of MBs at a mechanical index of

FIGURE 1 BP and Vascular Mechanical Properties

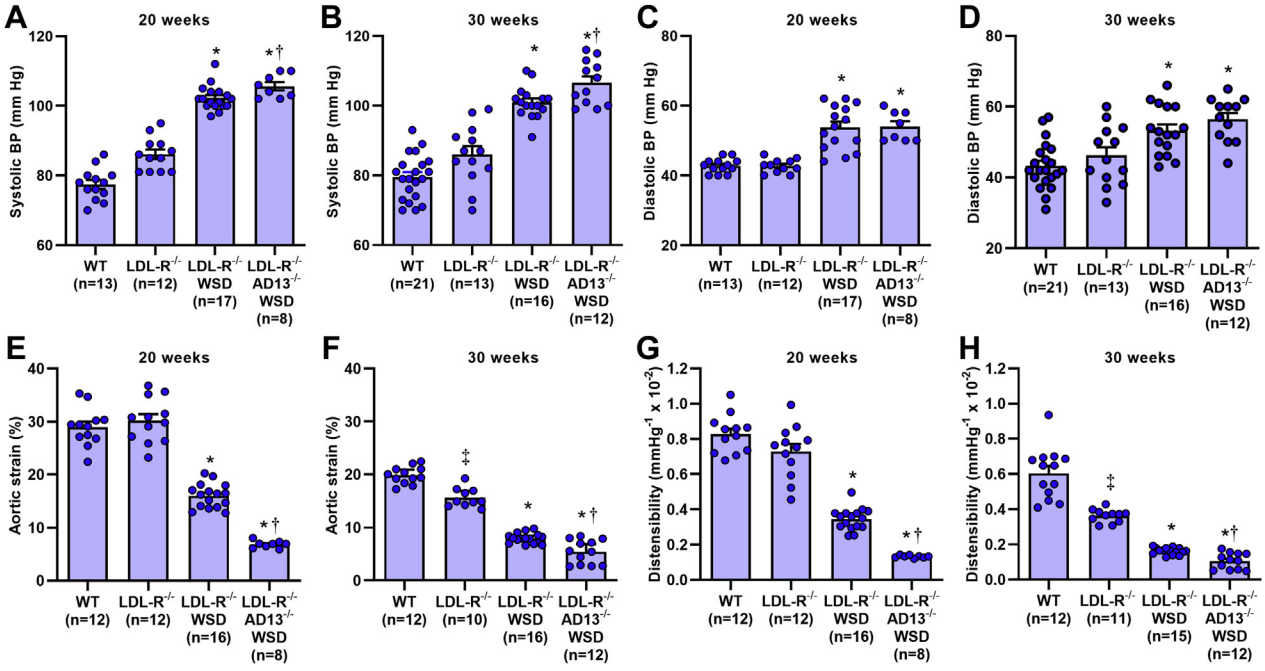

Systolic **(A,B)** and diastolic **(C,D)** blood pressure (BP) measured by awake tail cuff readings at 20 and 30 weeks of age. Aortic strain measured at the mid-ascending aorta by high-frequency ultrasound at 20 **(E)** and 30 **(F)** weeks of age. Aortic distensibility measured at the mid-ascending aorta at 20 **(G)** and 30 **(H)** weeks of age. Values are mean ± SEM. *$p < 0.05$ versus wild-type (WT) mice and mice deficient for low-density lipoprotein receptor (LDL-$R^{-/-}$); †$p < 0.05$ versus LDL-$R^{-/-}$ on a Western-style diet (WSD); ‡$p < 0.05$ versus WT mice. All p values are post hoc (analysis of variance, $p < 0.05$) analysis with unpaired Student's t-tests. $AD13^{-/-}$ = deficient for ADAMTS13.

1.5 representing signal from any residual freely circulating MBs (19). Regions of interest were standardized encompassing the aorta from the sinuses to the proximal arch just beyond the origin of the brachiocephalic artery. Data for each actively targeted agent was expressed as intensity beyond background signal obtained with control agent (MB). To avoid excessive volume administration, animals received only 3 agents (inclusive of control MBs) at each imaging session; the sections were randomly assigned to each animal and study interval.

BLOOD PRESSURE. Blood pressure (BP) was measured (n = 12 to 21 in each group) using a tail cuff plethysmograph (IITC Life Science Inc., Woodland Hills, California) in a designated quiet room. Mice were habituated for ≥7 days prior to BP measurement by allowing their spontaneous entry into the restrainer and adjusting tube length to limit motion. The cuff was placed at the base of the tail. System temperature was set at 34°C. Three measurements were acquired and averaged.

AORTIC DISTENSIBILITY. The diameter of the mid-ascending aorta at end-systole and end-diastole was measured (n = 11 to 15 in each group) by high-frequency (30 MHz) transthoracic B-mode and M-mode ultrasound imaging (Vevo2100, VisualSonics Inc., Toronto, Canada). Aortic distensibility was calculated by dividing aortic strain (proportional increase in diameter from diastole to systole) by the pulse pressure.

ARTERIAL NFκB. The descending thoracic aorta from 30-week-old mice was dissected free and homogenized in cold extraction buffer. An enzyme-linked immunosorbent assay was used to assess nuclear factor κ-light-chain-enhancer of activated B cells (NFκB) p65 subunit (pS536, Abcam, Cambridge, United Kingdom) in the supernatant as a transcriptomic marker of oxidative- and cytokine-mediated inflammation. Data were normalized to tissue weight.

HISTOLOGY. Histology was performed on 30-week-old mice, including those treated for 14 days with ADAMTS13 (n = 6 for each group). Blood was removed from the arterial system by infusion of isothermic phosphate-buffered saline containing 2.5% bovine serum albumin after which the aorta was perfusion-

FIGURE 2 **Molecular Imaging for vWF, Platelet Adhesion, and Endothelial Cell Adhesion Molecules**

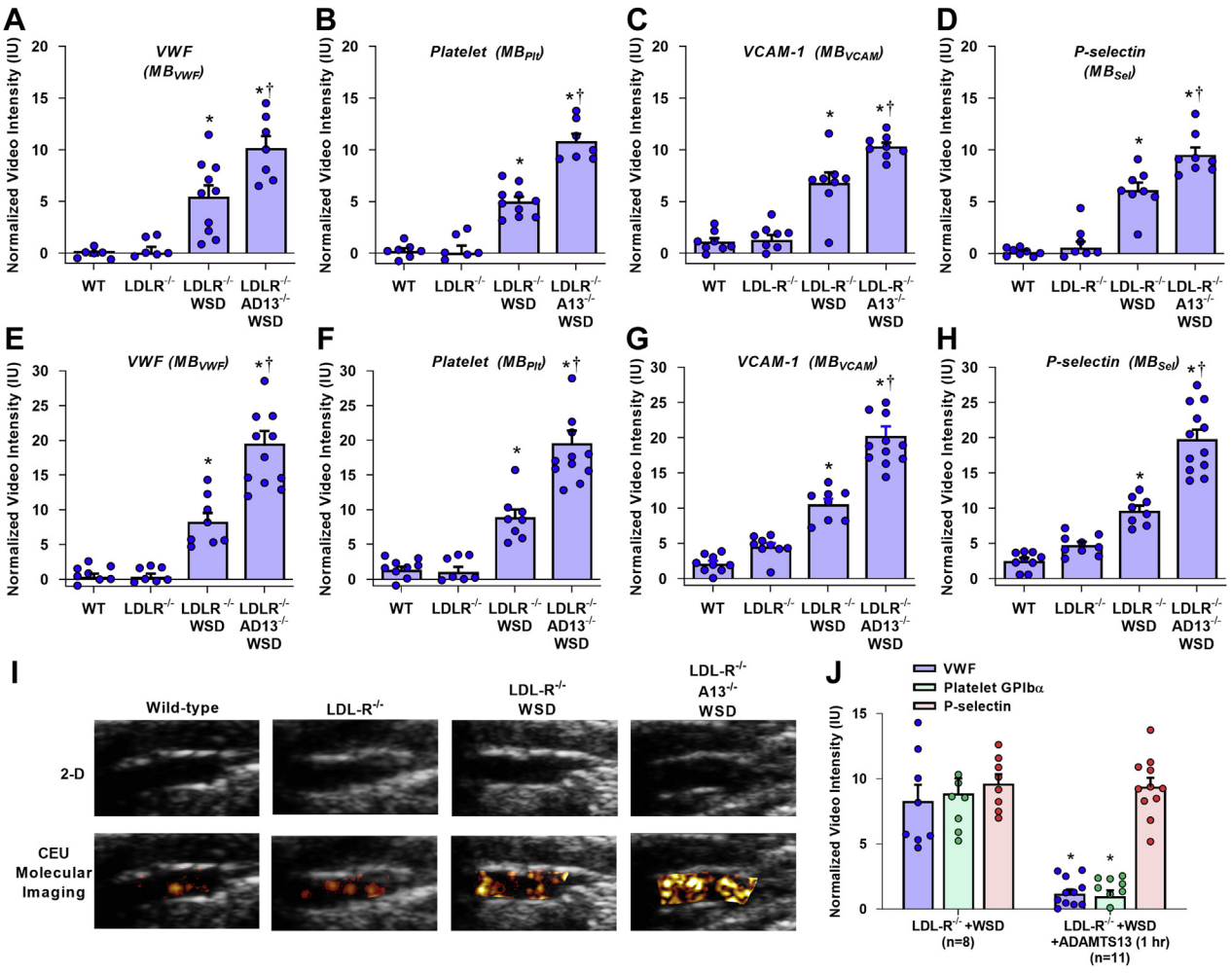

Signal enhancement was measured from the proximal thoracic aorta on contrast-enhanced ultrasound molecular imaging for von Willebrand factor (vWF), platelet glycoprotein Ibα (GPIbα) VCAM1, and P-selectin at either 20 **(A to D)** or at 30 **(E to H)** weeks of age. Normalized signal is quantified as that beyond what was obtained within the same animal with control, nontargeted agent. Values are mean ± SEM. *$p < 0.05$ versus WT and LDL-R$^{-/-}$; †$p < 0.05$ versus LDL-R$^{-/-}$ on WSD. The numbers of animals for each animal cohort, age, and contrast agent is provided in Supplemental Table 2. **(I)** Example of 2-dimensional transthoracic ultrasound B-mode imaging of the ascending aorta (caudal to the left) and superimposed background-subtracted color-coded molecular imaging for platelet GPIbα within a typical region of interest, for a 30-week-old LDL-R$^{-/-}$ mouse on WSD. **(J)** Signal enhancement measured from the proximal thoracic aorta on contrast-enhanced ultrasound molecular imaging for vWF, platelet GPIbα, and P-selectin in 20-week-old LDL-R$^{-/-}$ mice on WSD without or with ADAMTS13 (5 μg, intravenously) given1 h prior to imaging. *$p < 0.05$ versus untreated. All p values are post hoc (analysis of variance, $p < 0.05$) analysis with unpaired Student's t-tests. IU = international units; MB = microbubble; MB_{Plt} = microbubbles targeted to platelet adhesion; MB_{Sel} = microbubbles targeted to P-selectin; MB_{VCAM} = microbubbles targeted to VCAM1; MB_{vWF} = microbubbles targeted to endothelial von Willebrand factor; other abbreviations as in Figure 1.

fixed. Transaxial sections of the aortic root and the proximal descending thoracic aorta were stained with Masson trichrome stain to assess the plaque area defined by the tissue area within the internal elastic lamina and plaque collagen content. Immunohistochemistry was performed with rat anti-mouse primary monoclonal antibody against Mac-2 (M3/38, Thermo Fisher Scientific, Waltham, Massachusetts) for macrophages and dendritic cells, against CD41 (ab33661, Abcam) for platelets, and against vWF (ab6994, Abcam). Secondary staining was performed with species-appropriate secondary ALEXA Fluor-488-labeled Ab (Invitrogen, Grand Island, New York), Cy3-labeled (Jackson Immuno Research, West Grove, Pennsylvania) polyclonal antibody, or ALEXA Fluor-568-labeled polyclonal antibody (Invitrogen). Fluorescent microscopy was performed on a confocal system (TCS SP5, Leica Microsystems, Buffalo Grove,

FIGURE 3 Effect of AD13 on Molecular Imaging Signal

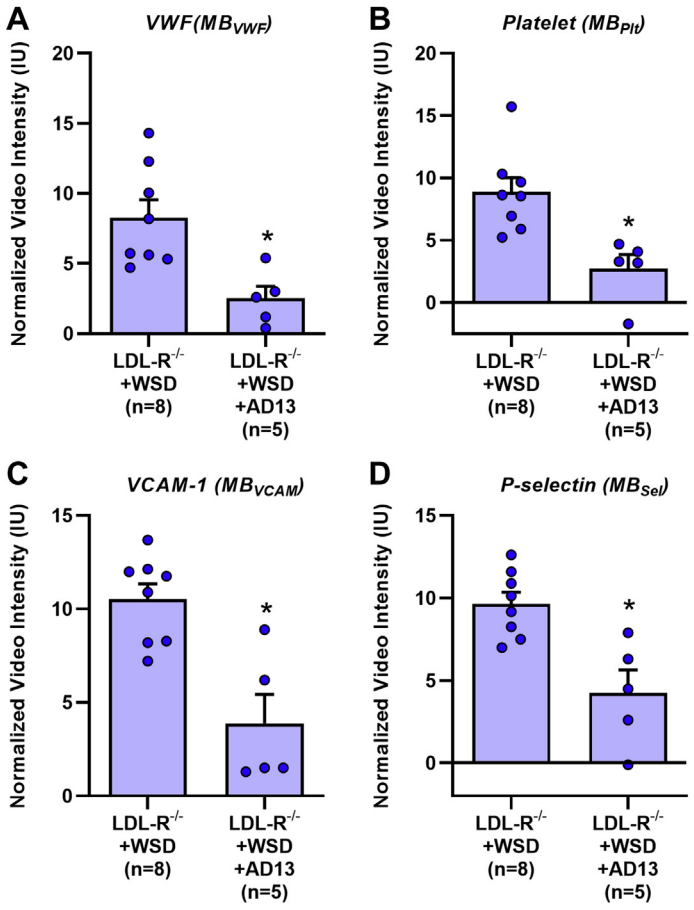

Signal enhancement was measured from the proximal thoracic aorta on contrast-enhanced ultrasound molecular imaging for vWF **(A)**, platelet GPIbα **(B)**, VCAM1 **(C)**, and P-selectin **(D)** at 30 weeks of age for LDL-R$^{-/-}$ mice on WSD with or without treatment for the prior 14 days with ADAMTS13 (AD13) administered by osmotic minipump. Values are mean ± SEM. *p < 0.05 versus LDL-R$^{-/-}$ on WSD by nonpaired Student's t-test. Abbreviations as in Figures 1 and 2.

Illinois). Spatial extent of plaque size, collagen content, Mac-2, and CD41 were quantified using Image-J software (National Institutes of Health, Bethesda, Maryland).

STATISTICAL ANALYSIS. Statistical analyses were performed using SPSS Statistics (version 25.0, IBM Corp., Armonk, New York). Continuous variables that were normally distributed area displayed as mean ± SD in tables and mean ± SEM in graphs. Tests for normal versus non-normal distribution were made using Shapiro-Wilk test. Student's *t*-test was performed for comparisons of normally distributed data. For multiple comparisons, 1-way analysis of variance was performed for normally distributed data with post hoc testing with Bonferroni correction. Correlations were made using linear regression and a Spearman rho test. Differences were considered significant at $p < 0.05$.

RESULTS

PLASMA LIPIDS, BP, AND AORTIC MECHANICAL PROPERTIES. Plasma lipid analysis demonstrated as stepwise increase in total cholesterol, LDL cholesterol, and triglycerides for wild-type mice, LDL-R$^{-/-}$ mice on normal chow, and LDL-R$^{-/-}$ mice on WSD (Table 1). Lipid profiles were similar between LDL-R$^{-/-}$ mice on WSD and LDL-R$^{-/-}$AD13$^{-/-}$ mice on WSD. In the animal groups with elevated plasma lipids, there was a high proportion of cholesterol that was in non-high-density lipoprotein and non-LDL fractions. There were no significant groupwise differences for complete blood count data or serum markers of renal function (Supplemental Table 1).

Systolic BP and diastolic BP were similar between wild-type and LDL-R$^{-/-}$ mice on chow diet at 20 and 30 weeks of age (Figures 1A to 1D). Compared with these 2 groups, LDL-R$^{-/-}$ mice on WSD and LDL-R$^{-/-}$AD13$^{-/-}$ mice on WSD had significantly higher systolic and diastolic BPs. Within each of the 4 groups, systolic and diastolic BPs were not significantly different at 20 versus 30 weeks of age. Aortic systolic strain and aortic distensibility at 20 weeks were similar between wild-type and LDL-R$^{-/-}$ mice on chow diet, whereas stepwise reductions in strain and distensibility were observed in LDL-R$^{-/-}$ on WSD and LDL-R$^{-/-}$AD13$^{-/-}$ on WSD (Figures 1E and 1G). The reduction in distensibility in LDL-R$^{-/-}$AD13$^{-/-}$ was severe, reaching 80% reduction when compared with reduction in wild-type mice. Similar patterns were seen at 30 weeks of age except aortic strain and distensibility were significantly lower in chow-fed LDL-R$^{-/-}$ than in wild-type mice (Figures 1F and 1H). There was an age-related reduction ($p < 0.05$) in distensibility between 20 and 30 weeks of age in all groups except the LDL-R$^{-/-}$AD13$^{-/-}$ mice who had severely impaired distensibility by 20 weeks of age.

ENDOTHELIAL vWF, PLATELET ADHESION, AND ADHESION MOLECULE EXPRESSION. On contrast-enhanced ultrasound molecular imaging, aortic endothelial signal for vWF, platelet GPIbα, VCAM1, and P-selectin were uniformly low in wild-type and LDL-R$^{-/-}$ mice on chow diet at 20 weeks of age (Figures 2A to 2D), and at 30 weeks of age (Figures 2E to 2I); although at 30 weeks, LDL-R$^{-/-}$ mice had slightly higher VCAM1 and P-selectin signals than in the wild-type mice. In LDL-R$^{-/-}$ mice, WSD resulted in a significantly higher molecular imaging signal for all vascular targets at both 20 weeks of age and

FIGURE 4 **Histology From the Aortic Root**

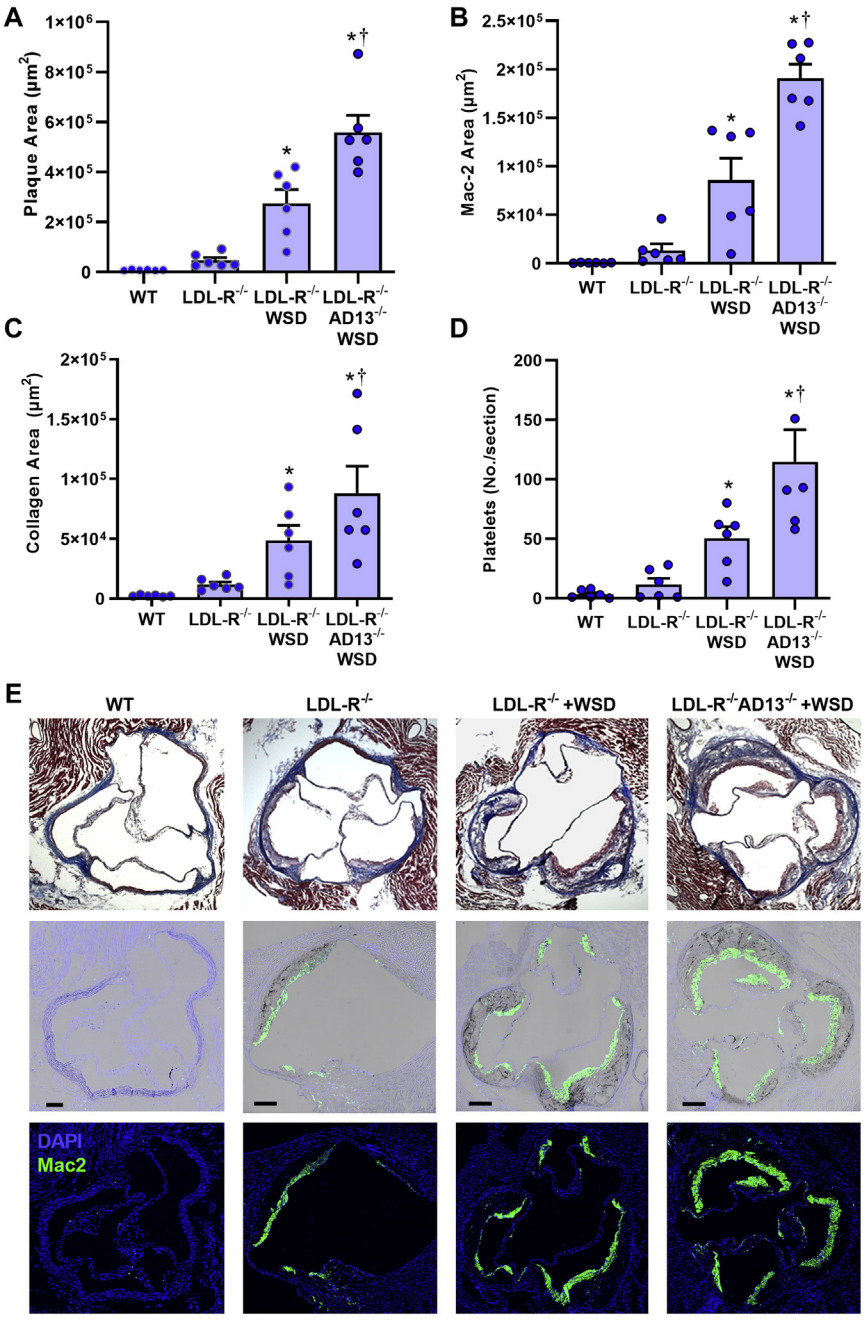

Histology at the level of the aortic sinuses at 30 weeks of age that include quantitative measurement of plaque area on Masson trichrome staining **(A)**, plaque macrophage area by Mac-2 staining **(B)**, plaque collagen area by Masson trichrome **(C)**, and platelet number by CD41 staining **(D)** seen per aortic root section. Values are mean ± SEM. *$p < 0.05$ versus WT and LDL-R$^{-/-}$; †$p < 0.05$ versus LDL-R$^{-/-}$ on WSD; ‡$p < 0.05$ versus WT mice. All p values are post hoc (analysis of variance, $p < 0.05$) analysis with unpaired Student's t-tests. $n = 6$ for each animal group. **(E)** Examples illustrating group-related differences in histology from the aortic root showing plaque area by Masson trichrome **(top row)**, fluorescent immunohistochemistry for Mac-2 **(bottom row)**, and merged bright-field and Mac-2 **(center row)**. Bars = 150 μm. DAPI = 4′,6-diamidino-2-phenylindole; other abbreviations as in Figure 1.

FIGURE 5 Correlation Between Arterial Phenotype on Molecular Imaging and Histology

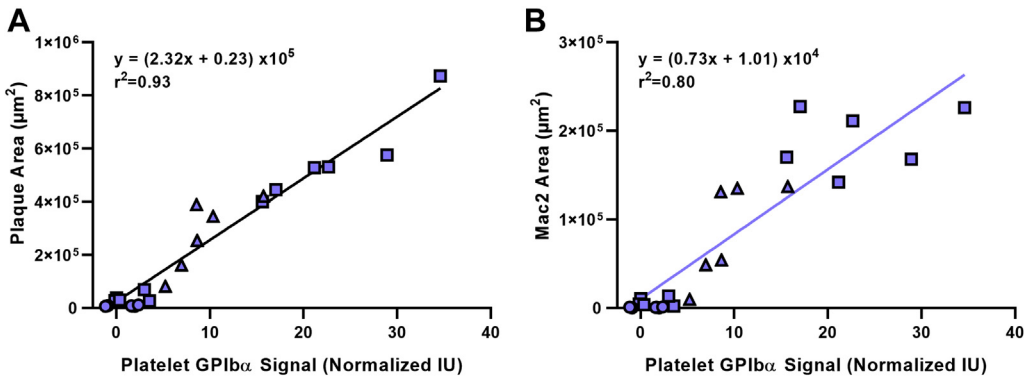

Correlations between contrast-enhanced ultrasound molecular imaging signal for platelet GPIbα and either plaque area **(A)** or plaque Mac-2 **(B)** on histology from the aortic sinuses at 30 weeks of age. Data are from all histological samples; **circles** represent WT mice; **open squares** represent LDL-R$^{-/-}$ mice; **triangles** represent LDL-R$^{-/-}$ mice on WSD; and **solid squares** represent LDL-R$^{-/-}$ AD13$^{-/-}$ mice on WSD. Abbreviations as in Figures 1 and 2.

30 weeks of age, consistent with an atherogenic endothelial phenotype. Compared with LDL-R$^{-/-}$ mice on WSD, LDL-R$^{-/-}$AD13$^{-/-}$ mice on WSD had even greater aortic signal enhancement at 20 and 30 weeks not only for vWF and platelet adhesion, but also for VCAM1 and P-selectin. In LDL-R$^{-/-}$ mice on WSD and LDL-R$^{-/-}$AD13$^{-/-}$ mice on WSD, signal enhancement for vWF, platelet GPIbα, VCAM1, and P-selectin significantly increased between 20 and 30 weeks of age ($p < 0.05$ for all targets). Aortic NFκB p65, which transcriptionally regulates expression of many endothelial cell adhesion molecules, was similar for wild-type and LDL-R$^{-/-}$ mice at 30 weeks of age, but increased in a stepwise manner in LDL-R$^{-/-}$ mice on WSD (9-fold increase vs. wild-type) and LDL-R$^{-/-}$AD13$^{-/-}$ mice on WSD (18-fold increase vs. wild-type) (Supplemental Figure 1).

Intravenous administration of recombinant ADAMTS13 was performed 1 h prior to molecular imaging in LDL-R$^{-/-}$ mice on WSD at 30 weeks of age using a dose that is expected to increase plasma concentration 6- to 8-fold. Treatment with ADAMTS13 almost completely eliminated signal for vWF and for platelet GPIbα, but not P-selectin (Figure 2J), indicating that excess endothelial-associated vWF was responsible for platelet adhesion in atherosclerotic mice even with intact ADAMTS13, and that most P-selectin signal was derived from the activated endothelium rather than from platelets. In contrast, continuous administration of ADAMTS13 by minipump for 14 days in LDL-R$^{-/-}$ mice on WSD (30 weeks of age) resulted in significant reductions in not only vWF and platelet GPIbα, but also for P-selectin and VCAM1 (Figure 3).

PLAQUE MORPHOLOGY AND CONTENT. At 30 weeks of age, there was no detectable aortic root plaque in wild-type mice (Figure 4). LDL-R$^{-/-}$ mice on chow had mild plaque formation while LDL-R$^{-/-}$ mice on WSD had a 5-fold larger plaque area ($p < 0.01$). Plaque area in LDL-R$^{-/-}$AD13$^{-/-}$ mice on WSD was 2-fold higher than LDL-R$^{-/-}$ mice on WSD. Proportionally similar increases in macrophage area, collagen area, and number of platelets associated with the plaque by CD41 staining were seen in LDL-R$^{-/-}$ on chow diet, LDL-R$^{-/-}$ on WSD, and LDL-R$^{-/-}$AD13$^{-/-}$ on WSD (Figures 4B to 4E). Platelets were observed not only directly adherent to the luminal plaque surface but also occasionally within the plaque core (Supplemental Figure 2). While immunohistochemistry for vWF is limited by its inability to discriminate which is surface-associated versus stored within endothelial Weibel-Palade bodies, there was, nonetheless, evidence for greater endothelial vWF staining overlying plaque in animals on WSD (Supplemental Figure 3). Histology from the descending aorta demonstrated similar groupwise differences in plaque size, macrophage content, collagen content, and platelet adhesion (Supplemental Figures 4 and 5). When examining the relationship between plaque histological features at 30 weeks of age and molecular imaging of the endothelium on contrast-enhanced ultrasound, a close linear relationship was found between platelet GPIbα signal and both plaque size and plaque macrophage content (Figure 5).

In 30-week-old LDL-R$^{-/-}$ mice on WSD, continuous treatment with ADAMTS13 for 2 weeks prior to study resulted in a significant reduction in plaque area and

FIGURE 6 Histologic Changes Produced by AD13 Treatment

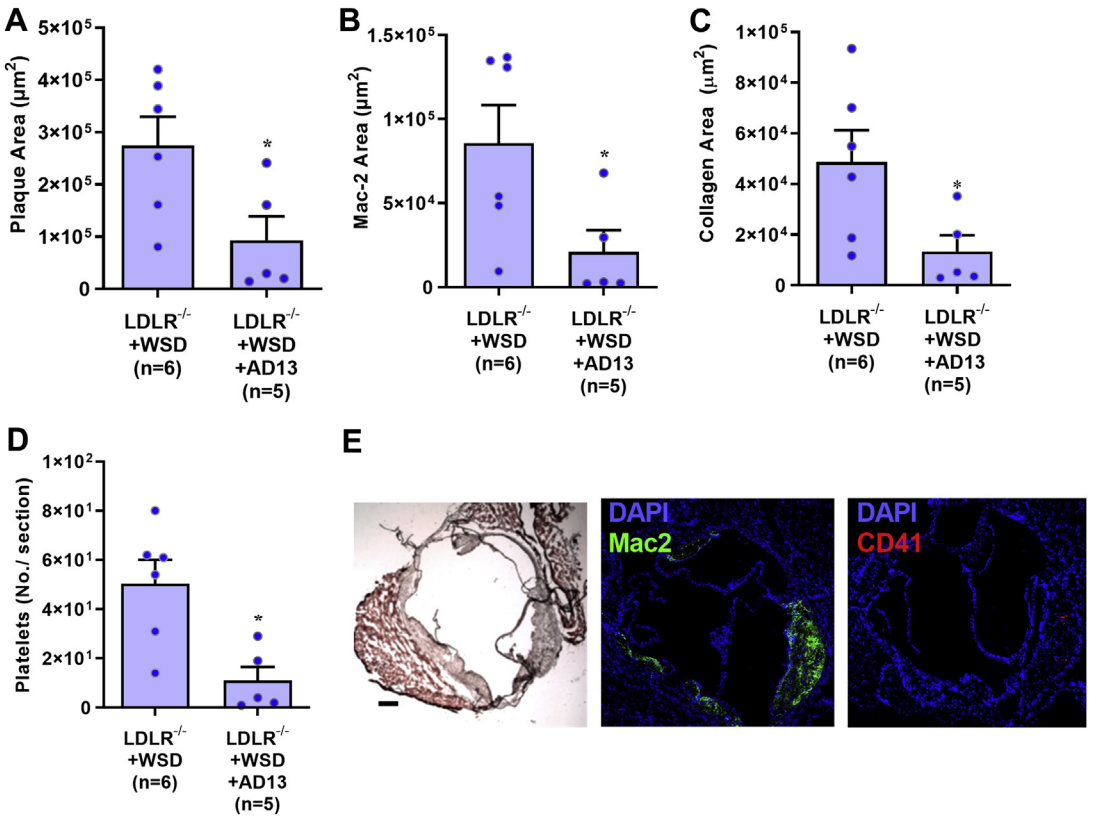

Histology from the aortic root at the level of the aortic sinuses in LDL-R$^{-/-}$ on WSD at 30 weeks of age comparing untreated and AD13-treated (2 weeks by osmotic minipump), include quantitative measurement of plaque area on Masson trichrome staining **(A)**, plaque macrophage area by Mac-2 staining **(B)**, plaque collagen area by Masson trichrome **(C)**, and platelet number by CD41 staining **(D)** seen per aortic root section. Values are mean ± SEM. *$p < 0.05$ versus WT and LDL-R$^{-/-}$ by unpaired Student's t-tests. $n = 6$ for each animal group. **(E)** Examples illustrating Masson trichrome **(left)**, fluorescent immunohistochemistry for Mac-2 **(center)**, and CD41 for platelets **(right)** are shown for comparison to **Figure 4**. Bars = 150 μm. Abbreviations as in **Figures 1, 3, and 4**.

proportional reductions in both Mac-2 area and platelet adhesion (**Figure 6**). There was also a reduction in the extent of vWF staining (Supplemental Figure 3).

DISCUSSION

Since the initial observations of platelet attachment to the intact endothelial surface in animal models of early atherosclerosis (5,20), there has been increasing interest in the role of platelets in the provocation of plaque development at various stages of disease. Preclinical mechanistic studies have indicated that vWF-mediated endothelial adhesion of platelets through GPIbα ligation occurs in atherosclerosis and is probably an important contributor to atherogenesis (3). In cross-sectional clinical studies, young subjects with symptomatic atherosclerosis have lower ADAMTS13 levels and higher vWF levels than in matched control subjects (21). Furthermore, prospective studies in older subjects have found that low ADAMTS13 activity is associated with cardiovascular-related mortality (22). Yet, in large trials of subjects with atherosclerotic risk factors, circulating levels of vWF are only modestly associated with future risk of atherosclerotic disease (22,23), possibly indicating that circulating plasma vWF does not necessarily reflect what occurs at the endothelial surface. For this reason, we have used contrast-enhanced ultrasound molecular imaging to examine events at the endothelial-blood pool interface to study vWF and platelet adhesion in atherosclerosis. Molecular imaging performed in murine models of diet- and age-related atherosclerosis demonstrated that the following: 1) endothelial-associated vWF with exposed A1 domain and secondary platelet adhesion

increase with disease severity in concert with changes in endothelial cell adhesion molecule expression (VCAM1, P-selectin); and 2) the increase in platelet adhesion in atherosclerotic mice deficient for ADAMTS13 is associated with greater endothelial cell adhesion molecule expression, larger plaque development, higher vascular NFκB concentration, and severe vascular stiffness. We also demonstrated that sustained treatment with recombinant ADAMTS13 is associated with a significant reduction in endothelial cell adhesion molecule expression.

Interaction between the GPIbα component of the GPIb-IX-V receptor complex on platelets and the A1 domain of vWF is an essential part of normal hemostasis (24). Ultralarge multimerized vWF protomers are stored in the Wiebel-Palade bodies of endothelial cells. When they are released, a fraction become associated with the endothelial surface but are subject to proteolysis at the A2 domain by ADAMTS13 (25). A variety of atherosclerosis-related factors such as increased oxidative stress, inflammation, and low levels of high-density lipoproteins are associated with reduced ADAMTS13 activity or levels (26–28). In this study, molecular imaging using MB contrast agents that are approximately the size of platelets and that bear recombinant gain-of-function GPIbα demonstrated an increase in endothelial-associated vWF with both diet- (LDL-R$^{-/-}$ mice on WSD vs. chow) and age-related increases in atherosclerotic severity.

Endothelial-associated vWF putatively plays a role in atherogenesis by recruiting platelets to vascular surface. There are many mechanisms by which platelets can promote plaque activation, particularly through vascular inflammatory activation, oxidative capacity, and direct activation of the inflammasome complex (2,29,30). Platelet-derived secreted factors such as chemokines (C-C and C-X-C motif), interleukins (IL-1b, IL-8), and CD40L all have been implicated as contributors to thromboinflammation, and many of which contribute to upregulation of NFκB (3,4,31). It is biologically plausible to hypothesize that ligation of platelets to the endothelial surface can promote atherosclerosis in a "paracrine" fashion. Immobilized platelets also can provide an additional surface for the adhesion of leukocytes through a variety of adhesive interactions and are known to direct leukocytes to sites for extravasation in the microcirculation (32,33). In murine models of atherosclerosis, functional inhibition of platelet GPIbα or genetic deletion of either *GPIbα* or *vWF* reduce plaque size and macrophage content (5,14,15,34,35). Likewise, crossing atherosclerosis-prone mice deficient for apolipoprotein-E (Apo-E$^{-/-}$) with AD13$^{-/-}$ mice increases atherosclerotic plaque size and macrophage content (13).

In the current study, LDL-R$^{-/-}$ mice had the expected phenotype of plaque development in the aortic root and descending aorta. Plaque size and macrophage content were much greater when mice were fed a WSD. Molecular imaging of the atherosclerosis-prone region of the proximal thoracic aorta demonstrated that endothelial expression of VCAM1 and P-selectin, endothelial-associated vWF, and adherent platelets were also much greater when LDL-R$^{-/-}$ mice were fed a WSD irrespective of whether mice were studied at 20 weeks of age (6 weeks on WSD) or at 30 weeks of age (16 weeks on diet). These findings support the notion that endothelial vWF and platelet adhesion are associated with, and possibly contribute to, endothelial activation and accelerated growth of plaque with high-risk features.

AD13$^{-/-}$ mice were crossed with LDL-R$^{-/-}$ mice and placed on WSD in order to study modulation of endothelial vWF and GPIbα-mediated platelet adhesion. Similar to studies using an Apo-E$^{-/-}$ background, absence of ADAMTS13 in LDL-R$^{-/-}$ mice on WSD increased plaque size at 30 weeks. In vivo molecular imaging demonstrated that, compared with LDL-R$^{-/-}$ mice on WSD with intact ADAMTS13, LDL-R$^{-/-}$AD13$^{-/-}$ mice had not only greater signal enhancement at plaque-prone areas for vWF and platelets, but also 2-fold greater VCAM1 and P-selectin expression and higher vascular NFκB. These findings support a direct causative role of platelets in the proinflammatory endothelial processes that govern immune cell trafficking in atherosclerosis and are consistent with descriptions of arterial neutrophil adhesion in arteries of hyperlipidemic mice deficient in ADAMTS13 (13). To further evaluate the role of vWF-mediated platelet adhesion, LDL-R$^{-/-}$ mice on WSD were treated with recombinant ADAMTS13. Bolus administration resulted in an immediate reduction in endothelial vWF and platelet adhesion, but not P-selectin signal, whereas continuous administration of ADAMTS13 for a longer period of time substantially reduced endothelial VCAM1 and P-selectin, supporting a role of platelet adhesion in chronic endothelial adhesion molecule expression. The sustained treatment with ADAMTS13 also led to a substantial reduction in plaque size and macrophage content, similar to what has been described when platelet depletion is performed LDLR$^{-/-}$ mice that results in smaller plaque size, less platelet macrophage content, and a rebalancing away from proinflammatory macrophages (9). For our study, the causative link between reductions in adhesion molecule expression and plaque size in animals treated with ADAMTS13 cannot yet be made.

STUDY LIMITATIONS. It is possible that high levels of NFκB and endothelial cell adhesion molecule expression in LDL-R$^{-/-}$AD13$^{-/-}$ and LDL-R$^{-/-}$ mice may have not be a cause of plaque growth and inflammation, but instead be secondary to plaque macrophage enrichment from an alternative mechanism. An argument against this alternative hypothesis is that higher VCAM1 and selectin molecular imaging signals were found in LDL-R$^{-/-}$AD13$^{-/-}$ mice even early after initiation of the WSD (20 weeks). Moreover, selectin, VCAM1, and platelet signal were proportionally elevated in ADAMTS13-deficient animal to a similar degree at 20 and 30 weeks of age. Another limitation is that, while the specificity of ADAMTS13 for vWF is well established, an alternative function for the protease cannot be excluded. While NFκB was significantly higher in LDL-R$^{-/-}$AD13$^{-/-}$ mice than in other groups, this measurement was made for the entire vessel wall rather than from the endothelium alone. We did not attempt to identify any single platelet-mediated process responsible for endothelial activation because of the overwhelming evidence that the vascular inflammatory effects of platelets are multifactorial (2,3,6). There are also limitations of the animal model that should be considered. In humans, a description of excess endothelial-associated ultra-large vWF in atherosclerosis is still lacking because of the paucity of methods for detecting this phenomenon. While we have demonstrated that differences in vWF can be seen by immunohistochemistry, this approach does not discriminate surface-associated vWF in its "active state." Hence murine models where molecular imaging can be performed were used. Yet, murine models of atherosclerosis, including LDL-R$^{-/-}$ mice, have important differences from humans in terms of the lipid abnormalities and the location of the atherosclerotic lesions. Unlike humans with severe ADAMTS13 deficiency, AD13$^{-/-}$ mice do not have spontaneous thrombotic thrombocytopenia without additional insult (i.e., calcium ionophore or histamine), possibly because of relative low vWF plasma concentrations in C57Bl/6 mice. Whereas osmotic minipumps were used for sustained increases in ADAMTS13 levels, we did not measure systemic concentrations and instead relied on molecular imaging of the intended effect, a reduction in vWF signal, to indicate intended effect. Finally, in humans, the protective effect of inherited deficiencies in vWF production is unclear because small studies examining atherosclerotic lesion development have shown modest effect (36), whereas large registry studies have found large reduction in cardiovascular event rates (37). We believe this controversy does not necessarily dissuade from our conclusion that excess endothelial-associated vWF is proatherogenic.

CONCLUSIONS

In summary, our in vivo molecular imaging data together with histology indicate that vWF-mediated platelet adhesion leads directly to proinflammatory up-regulation of endothelial cell adhesion molecules that are critical for recruitment of monocytes and other leukocyte populations involved in atherogenesis. The implications of these findings are that any condition that interferes with ADAMTS13 regulation of endothelial vWF (i.e., high oxidative stress, lipid disorders, inflammation, infection) are likely to accelerate atherogenesis; whereas any therapies that enhance ADAMTS13 activity or that suppress vWF-GPIbα interaction may be protective.

AUTHOR RELATIONSHIP WITH INDUSTRY

This work was supported by grants R01-HL078610, R01-HL130046, and P51-OD011092 to Dr. Lindner; R35-HL145262 to Dr. Lopez; and R01-HL137991 to Dr. Chung from the National Institutes of Health. This work was also supported by grant 16SDG27520011 to Dr. Tavori from the American Heart Association, the Japanese Society for the Promotion of Science Overseas Research Fellowship to Dr. Ozawa, and the Manpei Suzuki Diabetes Foundation to Dr. Ozawa. Dr. Mueller is supported by National Institutes of Health training grant T32-HL094294. All other authors have reported that they have no relationships relevant to the contents of this paper to disclose.

ADDRESS FOR CORRESPONDENCE: Dr. Jonathan R. Lindner, Cardiovascular Division, UHN-62, Oregon Health and Science University, 3181 Southwest Sam Jackson Park Road, Portland, Oregon 97239. E-mail: lindnerj@ohsu.edu.

PERSPECTIVES

COMPETENCY IN MEDICAL KNOWLEDGE: Platelets play a role not only in late stage atherothrombotic complications of atherosclerosis, but also in pro-inflammatory signaling that triggers disease initiation and growth.

TRANSLATIONAL OUTLOOK: During atherogenesis, platelets are thought to contribute to activation of the innate immune system. This study provides further understanding of thromboinflammation by showing that excess vWF on the arterial endothelial surface and secondary platelet adhesion leads directly to the expression of endothelial cell adhesion molecules involved in monocyte recruitment. These findings are of clinical importance because they indicate that: 1) new precision-based atherosclerotic risk factors could be considered based on endothelial-associated vWF or on molecular imaging; and 2) new therapies targeted to platelet-vWF interaction or to augmenting vWF proteolysis could be used to arrest plaque development.

REFERENCES

1. Libby P, Ridker PM, Hansson GK. Inflammation in atherosclerosis: from pathophysiology to practice. J Am Coll Cardiol 2009;54:2129–38.

2. Rondina MT, Weyrich AS, Zimmerman GA. Platelets as cellular effectors of inflammation in vascular diseases. Circ Res 2013;112:1506–19.

3. Wu MD, Atkinson TM, Lindner JR. Platelets and von Willebrand factor in atherogenesis. Blood 2017;129:1415–9.

4. Huo Y, Schober A, Forlow SB, et al. Circulating activated platelets exacerbate atherosclerosis in mice deficient in apolipoprotein E. Nat Med 2003; 9:61–7.

5. Massberg S, Brand K, Gruner S, et al. A critical role of platelet adhesion in the initiation of atherosclerotic lesion formation. J Exp Med 2002; 196:887–96.

6. Weber C. Platelets and chemokines in atherosclerosis: partners in crime. Circ Res 2005;96: 612–6.

7. Gerdes N, Seijkens T, Lievens D, et al. Platelet CD40 exacerbates atherosclerosis by transcellular activation of endothelial cells and leukocytes. Arterioscler Thromb Vasc Biol 2016;36: 482–90.

8. Garshick MS, Tawil M, Barrett TJ, et al. Activated platelets induce endothelial cell inflammatory response in psoriasis via COX-1 (cyclooxygenase-2). Arterioscler Thromb Vasc Biol 2020;40:1340–51.

9. Barrett TJ, Schlegel M, Zhou F, et al. Platelet regulation of myeloid suppressor of cytokine signaling 3 accelerates atherosclerosis. Sci Transl Med 2019;11:eaax0481.

10. McCarty OJ, Conley RB, Shentu W, et al. Molecular imaging of activated von Willebrand factor to detect high-risk atherosclerotic phenotype. J Am Coll Cardiol Img 2010;3:947–55.

11. Liu Y, Davidson BP, Yue Q, et al. Molecular imaging of inflammation and platelet adhesion in advanced atherosclerosis effects of antioxidant therapy with NADPH oxidase inhibition. Circ Cardiovasc Imaging 2013;6:74–82.

12. Shim CY, Liu YN, Atkinson T, et al. Molecular imaging of platelet-endothelial interactions and endothelial von Willebrand factor in early and mid-stage atherosclerosis. Circ Cardiovasc Imaging 2015;8:e002765.

13. Gandhi C, Khan MM, Lentz SR, Chauhan AK. ADAMTS13 reduces vascular inflammation and the development of early atherosclerosis in mice. Blood 2012;119:2385–91.

14. Doddapattar P, Dhanesha N, Chorawala MR, et al. Endothelial cell-derived von Willebrand factor, but not platelet-derived, promotes atherosclerosis in apolipoprotein E-deficient mice. Arterioscler Thromb Vasc Biol 2018;38:520–8.

15. Methia N, Andre P, Denis CV, Economopoulos M, Wagner DD. Localized reduction of atherosclerosis in von Willebrand factor-deficient mice. Blood 2001;98:1424–8.

16. Gandhi C, Ahmad A, Wilson KM, Chauhan AK. ADAMTS13 modulates atherosclerotic plaque progression in mice via a vWF-dependent mechanism. J Thromb Haemost 2014;12:255–60.

17. Flood VH, Gill JC, Morateck PA, et al. Gain-of-function GPIb ELISA assay for vWF activity in the Zimmerman Program for the Molecular and Clinical Biology of VWD. Blood 2011;117: e67–74.

18. Lindner JR, Song J, Christiansen J, Klibanov AL, Xu F, Ley K. Ultrasound assessment of inflammation and renal tissue injury with microbubbles targeted to P-selectin. Circulation 2001;104:2107–12.

19. Lindner JR, Dayton PA, Coggins MP, et al. Noninvasive imaging of inflammation by ultrasound detection of phagocytosed microbubbles. Circulation 2000;102:531–8.

20. Theilmeier G, Michiels C, Spaepen E, et al. Endothelial von Willebrand factor recruits platelets to atherosclerosis-prone sites in response to hypercholesterolemia. Blood 2002;99:4486–93.

21. Bongers TN, de Bruijne EL, Dippel DW, et al. Lower levels of ADAMTS13 are associated with cardiovascular disease in young patients. Atherosclerosis 2009;207:250–4.

22. Sonneveld MA, Franco OH, Ikram MA, et al. Von Willebrand factor, ADAMTS13, and the risk of mortality: the Rotterdam study. Arterioscler Thromb Vasc Biol 2016;36:2446–51.

23. Spiel AO, Gilbert JC, Jilma B. von Willebrand factor in cardiovascular disease: focus on acute coronary syndromes. Circulation 2008;117: 1449–59.

24. Ruggeri ZM. Von Willebrand factor, platelets and endothelial cell interactions. J Thromb Haemost 2003;1:1335–42.

25. Dong JF, Moake JL, Nolasco L, et al. ADAMTS-13 rapidly cleaves newly secreted ultralarge von Willebrand factor multimers on the endothelial surface under flowing conditions. Blood 2002; 100:4033–9.

26. Cao WJ, Niiya M, Zheng XW, Shang DZ, Zheng XL. Inflammatory cytokines inhibit ADAMTS13 synthesis in hepatic stellate cells and endothelial cells. J Thromb Haemost 2008;6: 1233–5.

27. Chen J, Fu X, Wang Y, et al. Oxidative modification of von Willebrand factor by neutrophil oxidants inhibits its cleavage by ADAMTS13. Blood 2010;115:706–12.

28. Chung DW, Chen J, Ling M, et al. High-density lipoprotein modulates thrombosis by preventing von Willebrand factor self-association and subsequent platelet adhesion. Blood 2016; 127:637–45.

29. Nording HM, Seizer P, Langer HF. Platelets in inflammation and atherogenesis. Front Immunol 2015;6:98.

30. Rolfes V, Ribeiro LS, Hawwari I, et al. Platelets fuel the inflammasome activation of innate immune cells. Cell Rep 2020;31:107615.

31. von Hundelshausen P, Schmitt MM. Platelets and their chemokines in atherosclerosis-clinical applications. Front Physiol 2014;5:294.

32. Sreeramkumar V, Adrover JM, Ballesteros I, et al. Neutrophils scan for activated platelets to initiate inflammation. Science 2014;346: 1234–8.

33. Zuchtriegel G, Uhl B, Puhr-Westerheide D, et al. Platelets guide leukocytes to their sites of extravasation. PLoS Biol 2016;14: e1002459.

34. Zhou H, Ran Y, Da Q, et al. Defective association of the platelet glycoprotein Ib-IX complex with the glycosphingolipid-enriched membrane domain inhibits murine thrombus and atheroma formation. J Immunol 2016;197:288–95.

35. Koltsova EK, Sundd P, Zarpellon A, et al. Genetic deletion of platelet glycoprotein Ib alpha but not its extracellular domain protects from atherosclerosis. Thromb Haemost 2014;112: 1252–63.

36. van Galen KP, Tuinenburg A, Smeets EM, Schutgens RE. Von Willebrand factor deficiency and atherosclerosis. Blood Rev 2012;26: 189–96.

37. Seaman CD, Yabes J, Comer DM, Ragni MV. Does deficiency of von Willebrand factor protect against cardiovascular disease? Analysis of a national discharge register. J Thromb Haemost 2015; 13:1999–2003.

KEY WORDS atherosclerosis, molecular imaging, platelets, von Willebrand factor

APPENDIX For supplemental figures and tables, please see the online version of this paper.